Rapid Communications

Potential high-T_c superconductivity in $CaYH_{12}$ under pressure

Xiaowei Liang,[1] Aitor Bergara,[2,3,4] Linyan Wang,[1] Bin Wen,[1] Zhisheng Zhao,[1] Xiang-Feng Zhou,[1] Julong He,[1] Guoying Gao,[1,*] and Yongjun Tian[1]

[1]*Center for High Pressure Science, State Key Laboratory of Metastable Materials Science and Technology, Yanshan University, Qinhuangdao 066004, China*

[2]*Departmento de Física de la Materia Condensada, Universidad del País Vasco, UPV/EHU, 48080 Bilbao, Spain*

[3]*Donostia International Physics Center (DIPC), 20018 Donostia, Spain*

[4]*Centro de Física de Materiales CFM, Centro Mixto CSIC-UPV/EHU, 20018 Donostia, Spain*

(Received 3 November 2018; revised manuscript received 8 March 2019; published 25 March 2019)

The high-pressure phases and superconductivity of $CaYH_{12}$ have been explored by using a particle swarm optimization structure prediction methodology in combination with first-principles calculations. Our results show that $CaYH_{12}$ becomes stable with a cubic $Fd\bar{3}m$ structure above 170 GPa, where metal atoms form body-centered-cubic (bcc) lattices and hydrogens occupy all the tetrahedral interstices of these bcc lattices, completing sodalitelike cages. The electron-phonon coupling calculations indicate that the $Fd\bar{3}m$ structure is a potential high-temperature superconductor, with a calculated T_c of 258 K at 200 GPa. Our current study provides a possibility for searching new high-T_c superconductors in ternary hydrides.

DOI: 10.1103/PhysRevB.99.100505

Looking for room-temperature superconductivity remains one of the most important topics in condensed matter physics. As the lightest element, hydrogen has been extensively analyzed for its potential high-T_c superconductivity [1–10]. However, many theoretical and experimental studies indicate that extraordinary high pressures are required to metallize hydrogen. Even though metallic hydrogen has been recently reported to be observed at 495 GPa, it still remains highly controversial [10]. In 2004 Ashcroft [11] predicted that hydrogen-rich compounds might also become high-temperature superconductors but at much lower pressures than those required for hydrogen, due to the chemical "precompression" by alloying hydrogen with other elements. This prediction stimulated extensive research [12–37], and since then many hydrides have been predicted to become superconductors under high pressure with T_c values over 100 K [12–21]. Interestingly, these predictions have been recently confirmed, as hydrogen sulfide and lanthanum hydride have been experimentally observed to superconduct with critical temperatures above 200 K [22–26]. H_3S was first predicted to be stable in a cubic $Im\bar{3}m$ structure [16] with a remarkably high T_c of 204 K. These predictions were later experimentally confirmed by compressing a H_2S sample [22]. Different from the pure covalent structure of H_3S, another class of metal hydrides containing H clathrates were predicted with higher T_c values than that of H_3S. In these hydrides, $Im\bar{3}m$ CaH_6 [17] was first proposed with a T_c of 235 K at 150 GPa and then YH_6 [18] was predicted to have the same cubic $Im\bar{3}m$ structure with a T_c of 264 K at 120 GPa, where metal atoms form a bcc lattice, and hydrogens occupy all the tetrahedral interstices of the bcc lattice, forming a sodalitelike cage. Recently, Liu *et al.* [19] and Peng *et al.* [20] predicted separately that LaH_{10} and YH_{10} are stable in a cubic $Fm\bar{3}m$ structure with H_{32} cages under pressure. The estimated T_c values by both groups are 286 K (at 210 GPa) [19] and 288 K (at 200 GPa) [20] for LaH_{10}, while 326 K (at 250 GPa) [19] and 303 K (at 400 GPa) [20] for YH_{10}, respectively. Theoretical studies show that strong electron-phonon coupling (EPC) of these phases is closely related to the phonon modes of H-H bonds within the cages. Guided by these theoretical predictions, $Fm\bar{3}m$ LaH_{10} was subsequently synthesized by using laser-heated diamond anvil cell techniques at 170 GPa and 1000 K [24]. More recently, the superconducting transition of this clathrate lanthanum superhydride has been measured almost simultaneously by Somayazulu *et al.* [25] and Drozdov *et al.* [26] with T_c of about 260 and 250 K at 190 and 170 GPa, respectively. These exciting results have greatly encouraged us to further explore clathrate hydrogen-rich hydrides.

As we discussed above, CaH_6 was first predicted to be stable in the H-clathrate structure with a high T_c and then the same structure was later predicted in YH_6. However, a report on their synthesis is still missing. As we know, Ca and Y atoms have a similar atomic radius and electronegativity, which might prevent the H cages from collapsing and thus might maintain excellent superconductivity when we mix them together with H atoms. Thus, here we focus on exploring the crystal structures and superconductivity of the ternary hydride $CaYH_{12}$ under pressure. Simultaneously, this might also provide alternative routes to synthesize these kinds of hydrides, such as CaH_6 and YH_6.

In this Rapid Communication, we used a particle swarm optimization structural search combined with first-principles calculations to study the high-pressure phases and superconductivity of $CaYH_{12}$. Starting from the $Im\bar{3}m$ phase of CaH_6 and considering the substitution method for metal atoms, the *a priori* simplest structure for $CaYH_{12}$ would be $Pm\bar{3}m$. However, although this structure is also highly competitive, a very similar cubic $Fd\bar{3}m$ structure is predicted to be the most stable

*gaoguoying@ysu.edu.cn

one above 170 GPa. Interestingly, EPC calculations revealed that $Fd\bar{3}m$ $CaYH_{12}$ is a potential high-temperature superconductor with a T_c of 258 K at 200 GPa, which is slightly higher than those of CaH_6 and YH_6 at the same pressure.

Structure searches were performed using the particle swarm optimization technique as implemented in the CALYPSO code [38,39]. This method has successfully predicted the high-pressure structures of various systems [31,40,41]. Structural relaxations were based on density functional theory within the Perdew-Burke-Ernzerhof parametrization of the generalized gradient approximation [42] as implemented in the Vienna *ab initio* simulation package [43]. The EPC calculations of the $Fd\bar{3}m$ and $Pm\bar{3}m$ structures were performed with density functional perturbation theory with the QUANTUM ESPRESSO code [44], where ultrasoft pseudopotentials for Ca, Y, and H with a kinetic energy cutoff of 60 Ry were employed. The $7\times7\times7$ and $9\times9\times9$ q-point meshes in the first Brillouin zone were used in the EPC calculation for the $Fd\bar{3}m$ and $Pm\bar{3}m$ phases, respectively. Correspondingly, Monkhorst-Pack grids of $28\times28\times28$ and $36\times36\times36$ were used to ensure k-point sampling convergence with Gaussians of width 0.02 Ry.

Here, crystal structural predictions are performed for $CaYH_{12}$ at 10, 50, 100, 150, 200, 250, 300, and 350 GPa, respectively, with system sizes containing up to 2 formula units (f.u.) per simulation cell. Below 100 GPa, three structures, $P\bar{1}(1)$, $P\bar{1}(2)$, and $P1$ (Fig. S1 [45]), are predicted, where the hydrogen atoms exist both in the form of H_2 dimers and monoatomic H. The existence of H_2 dimers in these structures shows a trend to decomposition of $CaYH_{12}$ at low pressure (Fig. S2 [45]). At higher pressures, when we just consider 1 f.u. in the simulation cell, a cubic $Pm\bar{3}m$ phase is predicted to be stable above 200 GPa [Fig. 1(a)]. In this structure, Ca and Y atoms together form a bcc lattice, and hydrogen atoms occupy all the tetrahedral interstices of the bcc lattice forming a sodalitelike cage. Actually, this structure can be easily derived by a direct substitution of metal atoms in the predicted $Im\bar{3}m$ phase for CaH_6 and YH_6.

When extending the structural search to 2 f.u. in the simulation cell, a different cubic $Fd\bar{3}m$ structure is predicted to be the most stable one at 200 GPa [Fig. 1(b)]. Interestingly, both $Fd\bar{3}m$ and $Pm\bar{3}m$ are very similar. However, in the $Fd\bar{3}m$ structure, Ca alternates with Y in all the directions in the bcc lattice, which leads to a much bigger conventional cell ($Ca_8Y_8H_{96}$) than in $Pm\bar{3}m$ ($CaYH_{12}$). The first and second nearest H-H distances in $Fd\bar{3}m$ are 1.18 and 1.26 Å at 200 GPa (Fig. S3 [45]). Added electrons from the metal atoms will occupy antibonding orbitals of the H-H unit, elongating its bond length [17,18]. As it will be discussed below, the number of electrons transferred from the metal atoms considerably affects the H-H separation. In addition, several very competitive metastable $Cmmm$, $P2_1/m$, $Imma$, and $P4/nmm$ structures are also predicted (see Fig. S4 [45]). Interestingly, all these structures are based on bcc metal lattices and H clathrates.

Figure 1(c) shows the calculated enthalpy curves for the predicted structures with respect to the $Pm\bar{3}m$ phase as a function of pressure. The enthalpies of the decomposition to binary hydrides were also taken into account. As CaH_4 was predicted to be the most stable stoichiometry in the Ca-H system [17] below 150 GPa and YH_3 is the experimentally known yttrium hydride at lower pressure, we have considered $CaH_4(I4/mmm) + YH_3(Fm\bar{3}m) + H_2(C2/c)$ as a possible decomposition route. On the other hand, as above 150 GPa CaH_6 and YH_6 were calculated to become more stable than CaH_4 and YH_3 [18], respectively, the enthalpy decomposition to $CaH_6(Im\bar{3}m) + YH_6(Im\bar{3}m)$ was also presented in Fig. 1(c). $Fd\bar{3}m$ $CaYH_{12}$ becomes thermodynamically stable above 135 GPa. However, it is dynamically unstable below 170 GPa. In this intermediate-pressure range, the H clathrate in $Fd\bar{3}m$ becomes gradually distorted, as the $P2_1/c$ structure in Fig. S1(d) [45], and breaks down into messy configurations, so that much bigger unit cells are needed to predict the correct structures at this pressure, which goes beyond our current computational capabilities. Even though the most stable structure is uncertain, our results can still show $CaYH_{12}$ is stable with respect to $CaH_4 + YH_3 + H_2$ above 116 GPa at least (Fig. S2 [45]). Additionally, due to the low mass of the hydrogen atom, we have also considered the zero-point energy (ZPE) contribution, which might influence the stability of hydrogen-rich materials. After considering ZPE, $CaYH_{12}$

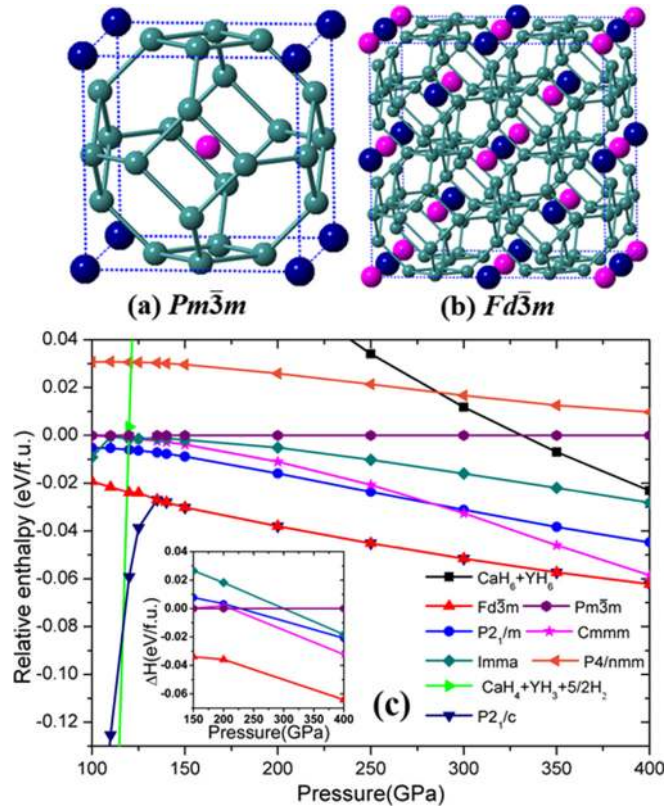

FIG. 1. The upper panel shows the predicted (a) $Pm\bar{3}m$ and (b) $Fd\bar{3}m$ structures of $CaYH_{12}$ at 200 GPa. The blue, magenta, and dark green atoms represent Ca, Y, and H atoms, respectively. The lower panel shows the calculated enthalpies per formula unit of various structures for $CaYH_{12}$ as a function of pressure with respect to the $Pm\bar{3}m$ structure. The decomposition enthalpies for $CaYH_{12}$ to $CaH_6(Im\bar{3}m) + YH_6(Im\bar{3}m)$ and $CaH_4(I4/mmm) + YH_3(Fm\bar{3}m) + H_2(C2/c)$ are also presented. Inset: Enthalpies of various structures relative to the $Pm\bar{3}m$ structure including zero-point corrections as a function of pressure.

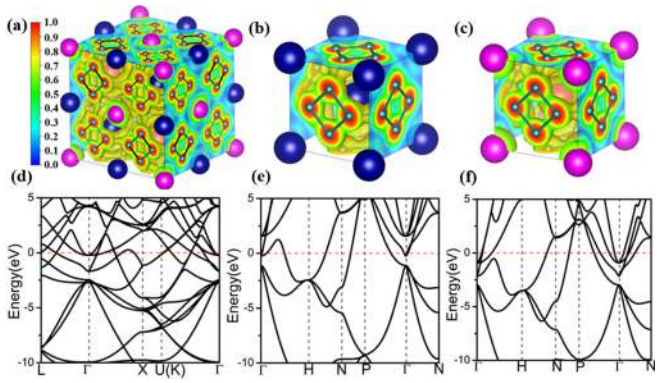

FIG. 2. ELF and electronic band structure. The calculated ELF of (a) $Fd\bar{3}m$ $CaYH_{12}$, (b) $Im\bar{3}m$ CaH_6, and (c) $Im\bar{3}m$ YH_6 with an isosurface value of 0.5 at 200, 150, and 120 GPa, respectively. The lower panels (d)–(f) show electronic band structures corresponding to the structures in the upper panel.

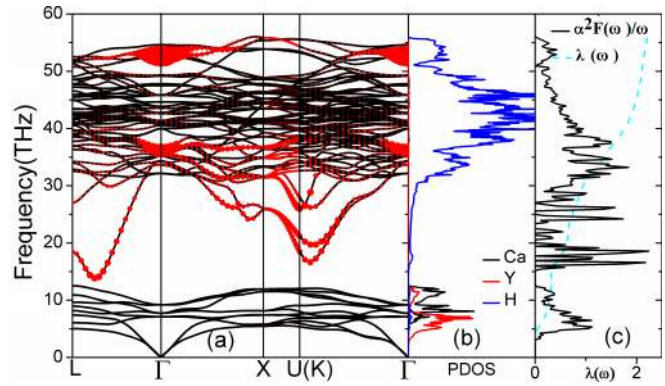

FIG. 3. Calculated phonon band structure for $Fd\bar{3}m$ $CaYH_{12}$ at 200 GPa (a). Red solid circles show the phonon linewidth with a radius proportional to the strength. (b) show Ca, Y, and H contributions to the phonon DOS. The Eliashberg phonon spectral function $\alpha^2F(\omega)$ and the partial electron-phonon integral $\lambda(\omega)$ are in (c).

starts to be thermodynamically stable at a lower pressure of about 106 GPa, which is lower than those required by CaH_6 and YH_6. Due to the uncertainty of low-pressure structures, we will center our next analysis in the higher-pressure range. From 170 to 400 GPa, the predicted $Fd\bar{3}m$ structure is the most stable one. Additionally, the ZPEs for the predicted structures at 150, 200, and 400 GPa were calculated within the quasiharmonic approximation [46]. According to our calculations, the $Fd\bar{3}m$ structure remains as the most stable one.

It is very complicated to construct the complete phase diagram for ternary hydrides, which is also beyond the reach of the current study. However, we have checked the stability of $CaYH_{12}$ relative to other possible ternary hydrides with different ratios of CaH_6 and YH_6. As shown in Fig. S5 [45], $CaYH_{12}$ is the most stable stoichiometry from 150 to 400 GPa. In addition, the current study also shows that there might exist other ternary hydrides with similar cubic structures, such as $Ca_5Y_3H_{48}$, Ca_3YH_{24}, and others.

As it is well known and has been experimentally observed, high temperature and high pressure usually promote the formation of hydrides with high H content and make them stable [24–26]. Thus, under high temperature and high pressure, $CaYH_{12}$ might be synthesized from the experimentally available materials $Ca + Y + H_2$ or $CaH_2 + YH_3 + H_2$.

To explore the bonding information, we calculated the electron localization functions (ELFs) [47,48] for the high-pressure structures of $CaYH_{12}$ [Fig. 2(a) and Fig. S6 [45]]. As shown in Fig. 2(a), the ELF values at the center of the shortest H-metal separations in the $Fd\bar{3}m$ structure are very low, showing there is no covalent bonding between them. The ELF values between hydrogen atoms are 0.64 and 0.56, indicating the existence of weak covalent bonds, which are consistent with those in $Im\bar{3}m$ CaH_6 and YH_6, respectively. As it is shown below, the difference in these ELF values comes from the different number of electrons accepted by the H-H bonds. One bond, marked with a black line (bond length of 1.18 Å and ELF value of 0.64), is adjacent to two Ca atoms and one Y, while the other one, marked with a dark green line (bond length of 1.26 Å and ELF value of 0.56), is close to one Ca atom and two Y. Subsequent Bader charge calculations [49] show that each Ca and Y atom donates 1 and 1.4 electrons to H atoms at 200 GPa, respectively. Therefore, one Ca and two Y atoms transfer more valence electrons to the H-H unit than two Ca and one Y, which results in a longer bond length and smaller ELF values of the H-H bond. In addition, the results of the crystal orbital Hamilton population (Fig. S7 [45]) are consistent with the ELF calculations.

The calculated electronic band structures for the $Fd\bar{3}m$ $CaYH_{12}$, $Im\bar{3}m$ CaH_6, and YH_6 are shown in Fig. 2. There are many bands crossing the Fermi level steeply in $Fd\bar{3}m$ $CaYH_{12}$, which reveals its metallic character. Moreover, there are also some flatter bands near the Fermi energy, associated with more localized electronic states, which might help to enhance the electron-phonon interaction [50]. Additionally, the electronic density of states (DOS) for both $Fd\bar{3}m$ and $Pm\bar{3}m$ $CaYH_{12}$ are shown in Fig. S8 [45]. Remarkably, hydrogen atoms have a large contribution to the DOS at the Fermi level, so that we might expect a strong electron-phonon interaction associated with hydrogen phonon modes.

To explore the superconductivity in $CaYH_{12}$, lattice phonons and EPC calculations were carried out for the $Fd\bar{3}m$ structure at 200 GPa (Fig. 3). We can clearly separate its phonon DOS into three regions. The low-frequency modes (0–8.5 THz) are associated with vibrations of heavy Y atoms, the intermediate-frequency branches (8.5–12.5 THz) are related to Ca atoms, and the high-frequency modes (12.5–56 THz) come mainly from H atoms. The calculated logarithmic average frequency $\omega_{\log}$ is 1230 K and the EPC parameter λ is 2.2 [(Fig. 3(c)], which is higher than that in YH_6 (1.88 at 200 GPa) (Table S1 [45]). This large λ mainly comes from the EPC of H modes (82%), especially from the isolated soft modes between 15 and 35 THz. With increasing pressure, these soft modes become harder [Fig. S11(d) [45]], while they are softened with decreasing pressure, until they become unstable below 170 GPa. When lowering the pressure the mechanical energy (PV) is not big enough to break the H_2 dimers [51], so that they can be formed and the predicted cagelike structures become gradually unstable. Interestingly, as can be seen in Fig. 3(a), besides the optical modes at around 35 and 52 THz at the Γ point, the soft modes between 15 and 35 THz show

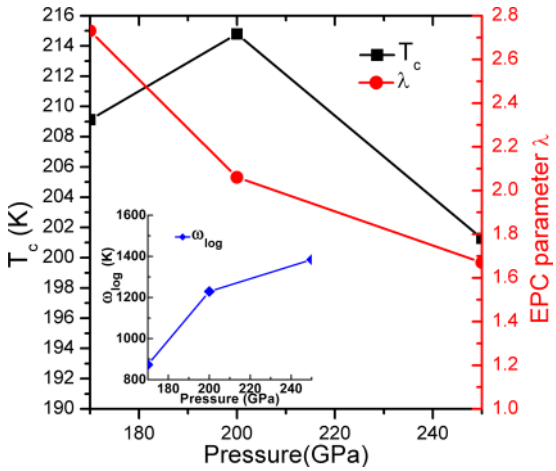

FIG. 4. Pressure dependence of T_c, calculated within the corrected Allen-Dynes modified McMillan equation, and the electron-phonon coupling parameter λ for the $Pm\bar{3}m$ structure. The inset shows the evolution of the logarithmic average frequency $\omega_{\log}$ with pressure.

a large phonon linewidth, with a high contribution to the Eliashberg spectral function $\alpha^2F(\omega)/\omega$ and λ. Similarly, the strong EPC in $Im\bar{3}m$ YH_6 is also closely associated with similar soft modes [18], while it is stemmed mostly from phonon modes (T_{2g} and E_g) at the Γ point in $Im\bar{3}m$ CaH_6 [17]. Therefore, the strong EPC in $Fd\bar{3}m$ $CaYH_{12}$ combines both cases of CaH_6 and YH_6. Similarly, a strong EPC with a λ of 2.06 is also estimated for the metastable $Pm\bar{3}m$ structure at 200 GPa [Fig. S9(f) [45]].

As the EPC parameter λ is larger than 1.5, in order to calculate T_c, the Allen-Dynes modified McMillan equation ($T_c = \frac{\omega_{\log}}{1.2}\exp[-\frac{1.04(1+\lambda)}{\lambda-\mu^*(1+0.62\lambda)}]$) needs to be corrected further by considering two separate correction factors (f_1 and f_2) ($T_c = \frac{f_1 f_2 \omega_{\log}}{1.2}\exp[-\frac{1.04(1+\lambda)}{\lambda-\mu^*(1+0.62\lambda)}]$) [52], where f_1 and f_2 represent the strong coupling and the shape correction, respectively. With a typical choice of the Coulomb pseudopotential μ^* of 0.1–0.3, the estimated T_c values for the $Fd\bar{3}m$ and $Pm\bar{3}m$ structures are 207–226 and 196–215 K at 200 GPa, respectively (Fig. S10 [45]). Actually, if T_c is further calculated by numerically solving the Eliashberg equation [53], they even increase a little, becoming 243–258 and 233–248 K, respectively. These predictions make $CaYH_{12}$ one of the few materials with a predicted T_c above 200 K. Moreover, the estimated T_c of the $Fd\bar{3}m$ $CaYH_{12}$ (243 K) is even somewhat higher than those of CaH_6 (201 K) [17] and YH_6 (233 K) at 200 GPa with μ^* of 0.13.

Considering the similarities between $Fd\bar{3}m$ and $Pm\bar{3}m$ $CaYH_{12}$ structures, and having in mind the complexity of the $Fd\bar{3}m$ structure makes the EPC calculations very time demanding, we have considered the $Pm\bar{3}m$ structure in order to analyze the pressure dependence of T_c. As it is shown in Fig. 4, the two main ingredients to estimate T_c, $\omega_{\log}$ and λ, present an opposite trend with pressure: $\omega_{\log}$ increases with pressure while λ decreases. Actually, this behavior can be easily understood in terms of the evolution with pressure of the intermediate soft modes we have described above. With increasing pressure these soft modes become stiffer (Fig. S9 [45]), which induces both a lowering on λ, as the Eliashberg spectral function is inversely proportional to the phonon frequency, and an increasing of $\omega_{\log}$. As a result of these two effects, the calculated T_c first increases with pressure and then decreases, reaching the highest value of 215 K at 200 GPa. Below 200 GPa, the value of λ is so high that, as T_c saturates with λ for high values of λ, $\omega_{\log}$ plays a major role on the evolution of T_c with pressure. Therefore, for pressures below 200 GPa, T_c follows the trend of $\omega_{\log}$, so that it increases with pressure. However, above 200 GPa, λ decreases with pressure and goes out of the saturation range, so that its evolution dominates over the increase of $\omega_{\log}$ with pressure. Therefore, above 200 GPa, T_c follows the trend of λ and decreases with pressure.

It is important to note that our calculations were based on the harmonic approximation, and the soft modes in the phonon spectra of $CaYH_{12}$ might be affected by anharmonic effects. Some studies, e.g., on AlH_3 [54], PdH [55], and PtH [56], show that anharmonicity strongly renormalizes the phonon frequencies and suppresses the λ. However, anharmonicity seems to have little effect on the EPC of pure hydrogen [8] and even can enhance it [57]. More importantly, the LaH_{10} clathrate was predicted to be a good superconductor with a T_c of 274–286 K at 210 GPa within the harmonic approximation [19], which is in good agreement with the recent experimental measurement of T_c 250–260 K [25,26]. Actually, the high-pressure clathrate structure of $CaYH_{12}$ and the phonon softening appearing in its phonon spectra are very similar to those of LaH_{10}. Therefore, according to our calculations, we believe that $CaYH_{12}$ is also a potential high-T_c superconductor.

In summary, we have extensively investigated the crystal structures and superconductivity of ternary hydride $CaYH_{12}$ under pressure. A cubic $Fd\bar{3}m$ structure is predicted to be stable above 170 GPa, where Ca and Y atoms together form a bcc lattice and hydrogen atoms adopt a clathrate structure, which retains the similar H-clathrate structures as $Im\bar{3}m$ CaH_6 and YH_6. More importantly, $CaYH_{12}$ is energetically favored relative to CaH_6 and YH_6 within a certain pressure range. Electron-phonon coupling calculations show that the cubic $Fd\bar{3}m$ $CaYH_{12}$ could be a high-T_c superconductor, with the highest one among the already studied ternary hydrides. Our findings might provide a possible route to synthesize hydrides such as CaH_6 and YH_6, and will further stimulate more theoretical and experimental studies on high-T_c superconductors in ternary hydrides.

The work was supported by National Natural Science Foundation of China (Grants No. 11604290 and No. 51732010), the Science Foundation for the Youth Top-notch Talent from Universities of Hebei Province (Grant No. BJ2017023), Funding Program for Recruited Oversea Scholars of Hebei Province (CL201729), and the Ph.D. Foundation by Yanshan University (Grant No. B970). A.B. acknowledges financial support from the Spanish Ministry of Economy and Competitiveness (FIS2016-76617-P) and the Department of Education, Universities and Research of the Basque Government and the University of the Basque Country (IT756-13).

[1] N. W. Ashcroft, Phys. Rev. Lett. **21**, 1748 (1968).
[2] A. F. Goncharov, E. Gregoryanz, R. J. Hemley, and H. Mao, Proc. Natl. Acad. Sci. USA **98**, 14234 (2001).
[3] P. Loubeyre, F. Occelli, and R. Letoullec, Nature (London) **416**, 613 (2002).
[4] C. J. Pickard and R. J. Needs, Nat. Phys. **3**, 473 (2007).
[5] L. Zhang, Y. Niu, Q. Li, T. Cui, Y. Wang, Y. Ma, Z. He, and G. Zou, Solid State Commun. **141**, 610 (2007).
[6] P. Cudazzo, G. Profeta, A. Sanna, A. Floris, A. Continenza, S. Massidda, and E. K. U. Gross, Phys. Rev. Lett. **100**, 257001 (2008).
[7] J. M. McMahon and D. M. Ceperley, Phys. Rev. B **84**, 144515 (2011).
[8] M. Borinaga, I. Errea, M. Calandra, F. Mauri, and A. Bergara, Phys. Rev. B **93**, 174308 (2016).
[9] P. Dalladay-Simpson, R. T. Howie, and E. Gregoryanz, Nature (London) **529**, 63 (2016).
[10] R. P. Dias and I. F. Silvera, Science **357**, 715 (2017).
[11] N. W. Ashcroft, Phys. Rev. Lett. **92**, 187002 (2004).
[12] X. Jin, X. Meng, Z. He, Y. Ma, B. Liu, T. Cui, G. Zou, and H.-k. Mao, Proc. Natl. Acad. Sci. USA **107**, 9969 (2010).
[13] G. Gao, H. Wang, A. Bergara, Y. Li, G. Liu, and Y. Ma, Phys. Rev. B **84**, 064118 (2011).
[14] S. Zhang, Y. Wang, J. Zhang, H. Liu, X. Zhong, H. F. Song, G. Yang, L. Zhang, and Y. Ma, Sci. Rep. **5**, 15433 (2015).
[15] X. Zhong, H. Wang, J. Zhang, H. Liu, S. Zhang, H.-F. Song, G. Yang, L. Zhang, and Y. Ma, Phys. Rev. Lett. **116**, 057002 (2016).
[16] D. Duan, Y. Liu, F. Tian, D. Li, X. Huang, Z. Zhao, H. Yu, B. Liu, W. Tian, and T. Cui, Sci. Rep. **4**, 6968 (2014).
[17] H. Wang, J. S. Tse, K. Tanaka, T. Iitaka, and Y. Ma, Proc. Natl. Acad. Sci. USA **109**, 6463 (2012).
[18] Y. Li, J. Hao, H. Liu, J. Tse, Y. Wang, and Y. Ma, Sci. Rep. **5**, 9948 (2015).
[19] H. Liu, I. I. Naumov, R. Hoffmann, N. W. Ashcroft, and R. J. Hemley, Proc. Natl. Acad. Sci. USA **114**, 6990 (2017).
[20] F. Peng, Y. Sun, C. J. Pickard, R. J. Needs, Q. Wu, and Y. Ma, Phys. Rev. Lett. **119**, 107001 (2017).
[21] X. Feng, J. Zhang, G. Gao, H. Liu, and H. Wang, RSC Adv. **5**, 59292 (2015).
[22] A. P. Drozdov, M. I. Eremets, I. A. Troyan, V. Ksenofontov, and S. I. Shylin, Nature (London) **525**, 73 (2015).
[23] M. Einaga, M. Sakata, T. Ishikawa, K. Shimizu, M. Eremets, A. Drozdov, I. Troyan, N. Hirao, and Y. Ohishi, Nat. Phys. **12**, 835 (2016).
[24] Z. M. Geballe, H. Liu, A. K. Mishra, M. Ahart, M. Somayazulu, Y. Meng, M. Baldini, and R. J. Hemley, Angew. Chem., Int. Ed. **57**, 688 (2018).
[25] M. Somayazulu, M. Ahart, A. K. Mishra, Z. M. Geballe, M. Baldini, Y. Meng, V. V. Struzhkin, and R. J. Hemley, Phys. Rev. Lett. **122**, 027001 (2019).
[26] A. P. Drozdov, P. P. Kong, V. S. Minkov, S. P. Besedin, M. A. Kuzovnikov, S. Mozaffari, L. Balicas, F. Balakirev, D. Graf, V. B. Prakapenka, E. Greenberg, D. A. Knyazev, M. Tkacz, and M. I. Eremets, arXiv:1812.01561.
[27] G. Gao, A. R. Oganov, A. Bergara, M. Martinez-Canales, T. Cui, T. Iitaka, Y. Ma, and G. Zou, Phys. Rev. Lett. **101**, 107002 (2008).
[28] T. Bi, N. Zarifi, T. Terpstra, and E. Zurek, *Reference Module in Chemistry, Molecular Sciences and Chemical Engineering* (Elsevier, Amsterdam, 2019), doi:10.1016/B978-0-12-409547-2.11435-0.
[29] G. Gao, A. R. Oganov, P. Li, Z. Li, H. Wang, T. Cui, Y. Ma, A. Bergara, A. O. Lyakhov, T. Iitaka, and G. Zou, Proc. Natl. Acad. Sci. USA **107**, 1317 (2010).
[30] K. Abe, Phys. Rev. B **96**, 144108 (2017).
[31] Y. Li, J. Hao, H. Liu, Y. Li, and Y. Ma, J. Chem. Phys. **140**, 174712 (2014).
[32] C. Kokail, W. von der Linden, and L. Boeri, Phys. Rev. Mater. **1**, 074803 (2017).
[33] G. Markopoulos, P. Kroll, and R. Hoffmann, J. Am. Chem. Soc. **132**, 748 (2010).
[34] T. Muramatsu, W. K. Wanene, M. Somayazulu, E. Vinitsky, D. Chandra, T. A. Strobel, V. V. Struzhkin, and R. J. Hemley, J. Phys. Chem. C **119**, 18007 (2015).
[35] M. Rahm, R. Hoffmann, and N. W. Ashcroft, J. Am. Chem. Soc. **139**, 8740 (2017).
[36] Y. Ma, D. Duan, Z. Shao, H. Yu, H. Liu, F. Tian, X. Huang, D. Li, B. Liu, and T. Cui, Phys. Rev. B **96**, 144518 (2017).
[37] Y. Ma, D. Duan, Z. Shao, D. Li, L. Wang, H. Yu, F. Tian, H. Xie, B. Liu, and T. Cui, Phys. Chem. Chem. Phys. **19**, 27406 (2017).
[38] Y. Wang, J. Lv, L. Zhu, and Y. Ma, Phys. Rev. B **82**, 094116 (2010).
[39] Y. Wang, J. Lv, L. Zhu, and Y. Ma, Comput. Phys. Commun. **183**, 2063 (2012).
[40] J. Lv, Y. Wang, L. Zhu, and Y. Ma, Phys. Rev. Lett. **106**, 015503 (2011).
[41] L. Zhu, H. Liu, C. J. Pickard, G. Zou, and Y. Ma, Nat. Chem. **6**, 644 (2014).
[42] J. P. Perdew, J. A. Chevary, S. H. Vosko, K. A. Jackson, M. R. Pederson, D. J. Singh, and C. Fiolhais, Phys. Rev. B **46**, 6671 (1992).
[43] G. Kresse and J. Furthmüller, Phys. Rev. B **54**, 11169 (1996).
[44] P. Giannozzi, S. Baroni, N. Bonini, M. Calandra, R. Car, C. Cavazzoni, D. Ceresoli, G. L. Chiarotti, M. Cococcioni, I. Dabo *et al.*, J. Phys.: Condens. Matter **21**, 395502 (2009).
[45] See Supplemental Material at http://link.aps.org/supplemental/10.1103/PhysRevB.99.100505 for computational details, predicted structures and calculated enthalpy curves at lower pressure, histogram of H-H distances in $Fd\bar{3}m$ $CaYH_{12}$, predicted metastable high-pressure structures, convex hull for different Ca-Y-H compounds, ELF and electronic band structures, density of states for $Fd\bar{3}m$ and $Pm\bar{3}m$ $CaYH_{12}$, $Im\bar{3}m$ CaH_6, and $Im\bar{3}m$ YH_6, superconductivity of the $Pm\bar{3}m$ structure as a function of pressure, calculated T_c values, and dynamical properties of $CaYH_{12}$ and structural information, which includes Refs. [17,42–44,49,58–62].
[46] Y. Ma and J. S. Tse, Solid State Commun. **143**, 161 (2007).
[47] A. D. Becke and K. E. Edgecombe, J. Chem. Phys. **92**, 5397 (1990).
[48] A. Savin, O. Jepsen, J. Flad, O. K. Andersen, H. Preuss, and H. G. von Schnering, Angew. Chem., Int. Ed. **31**, 187 (1992).
[49] R. Bader, *Atoms in Molecules: A Quantum Theory* (Oxford University Press, Oxford, UK, 1994).
[50] A. Simon, Angew. Chem., Int. Ed. **36**, 1788 (1997).
[51] K. Nagao, S. A. Bonev, A. Bergara, and N. W. Ashcroft, Phys. Rev. Lett. **90**, 035501 (2003).
[52] P. B. Allen and R. C. Dynes, Phys. Rev. B **12**, 905 (1975).

[53] G. M. Eliashberg, Zh. Eksp. Teor. Fiz. **38**, 966 (1960) [Sov. Phys. JETP **11**, 696 (1960)].
[54] B. Rousseau and A. Bergara, Phys. Rev. B **82**, 104504 (2010).
[55] I. Errea, M. Calandra, and F. Mauri, Phys. Rev. Lett. **111**, 177002 (2013).
[56] I. Errea, Eur. Phys. J. B **89**, 237 (2016).
[57] M. Borinaga, P. Riego, A. Leonardo, M. Calandra, F. Mauri, A. Bergara, and I. Errea, J. Phys.: Condens. Matter **28**, 494001 (2016).
[58] K. Parlinski, Z. Q. Li, and Y. Kawazoe, Phys. Rev. Lett. **78**, 4063 (1997).
[59] A. Togo, F. Oba, and I. Tanaka, Phys. Rev. B **78**, 134106 (2008).
[60] R. Dronskowski and P. E. Bloechl, J. Phys. Chem. **97**, 8617 (1993).
[61] V. L. Deringer, A. L. Tchougréeff, and R. Dronskowski, J. Phys. Chem. A **115**, 5461 (2011).
[62] S. Maintz, V. L. Deringer, A. L. Tchougréeff, and R. Dronskowski, J. Comput. Chem. **37**, 1030 (2016).